First-principles study of the structural, electronic, and magnetic properties of double perovskite Sr_2FeReO_6 containing various imperfections*

Yan Zhang(张研)[1,†], Li Duan(段理)[1], Vincent Ji[2], and Ke-Wei Xu(徐可为)[3]

[1] School of Materials Science and Engineering, Chang'an University, Xi'an 710061, China
[2] ICMMO/SP2M, UMR CNRS 8182, Université Paris-Sud, 91405 Orsay Cédex, France
[3] State Key Laboratory for Mechanical Behavior of Materials, Xi'an Jiaotong University, Xi'an 710049, China

(Received 15 December 2015; revised manuscript received 28 January 2016; published online 1 April 2016)

The structural, electronic, and magnetic properties of double perovskite Sr_2FeReO_6 containing eight different imperfections of Fe_{Re} or Re_{Fe} antisites, Fe1–Re1 or Fe1–Re4 interchanges, V_{Fe}, V_{Re}, V_O or V_{Sr} vacancies have been studied by using the first-principles projector augmented wave (PAW) within generalized gradient approximation as well as taking into account the on-site Coulomb repulsive interaction (GGA+U). No obvious structural changes are observed for the imperfect Sr_2FeReO_6 containing Fe_{Re} or Re_{Fe} antisites, Fe1–Re1 or Fe1–Re4 interchanges, or V_{Sr} vacancy defects. However, the six (eight) nearest oxygen neighbors of the vacancy move away from (close to) V_{Fe} or V_{Re} (V_O) vacancies. The half-metallic (HM) character is maintained for the imperfect Sr_2FeReO_6 containing Fe_{Re} or Re_{Fe} antisites, Fe1–Re4 interchange, V_{Fe}, V_O or V_{Sr} vacancies, while it vanishes when the Fe1–Re1 interchange or V_{Re} vacancy is presented. So the Fe1–Re1 interchange and the V_{Re} vacancy defects should be avoided to preserve the HM character of Sr_2FeReO_6 and thus usage in spintronic devices. In the Fe_{Re} or Re_{Fe} antisites, Fe1–Re1 or Fe1–Re4 interchanges cases, the spin moments of the Fe (Re) cations situated on Re (Fe) antisites are in an antiferromagnetic coupling with those of the Fe (Re) cations on the regular sites. In the V_{Fe}, V_{Re}, V_O, or V_{Sr} vacancies cases, a ferromagnetic coupling is obtained within each cation sublattice, while the two cation sublattices are coupled antiferromagnetically. The total magnetic moments μ_{tot} (μ_B/f.u.) of the imperfect Sr_2FeReO_6 containing eight different defects decrease in the sequence of V_{Sr} vacancy (3.50), V_{Re} vacancy (3.43), Fe_{Re} antisite (2.74), V_O vacancy (2.64), V_{Fe} vacancy (2.51), Re_{Fe} antisite (2.29), Fe1–Re4 interchange (1.96), Fe1–Re1 interchange (1.87), and the mechanisms of the saturation magnetization reduction have been analyzed.

Keywords: double perovskite, imperfections, electronic properties, magnetic properties

PACS: 81.05.Je, 71.55.Jv, 71.23.–k, 75.25.–j **DOI:** 10.1088/1674-1056/25/5/058102

1. Introduction

Over the past few decades, magnetic double perovskites with a general chemical formula of $A_2BB'O_6$, where A is an alkaline earth metal or rare earth metal cation, and B and B' are 3d and 4d/5d transition-metal (TM) cations, respectively, have been studied, especially the finding of the intrinsic tunneling magnetoresistance (TMR) effect at room temperature in Sr_2FeMoO_6[1] and Sr_2FeReO_6[2] revives the extensive study of the double perovskites $A_2BB'O_6$. Band-structure calculations reveal that they have a ferrimagnetic (FiM) half-metallic (HM) character with completely (100%) spin-polarized transport properties at the Fermi level.[1,2] The Curie temperatures T_C of Sr_2FeMoO_6 and Sr_2FeReO_6 are found to be fairly high, as high as 415 K and 401 K, respectively, making them potential candidates for industrial applications in magnetoresistive[3] and spintronics[4] devices at room temperature. Besides experimental works,[1,2,5–13] various first-principles methods[1,2,14–19] including the local spin density approximation (LSDA) and the generalized gradient approximation (GGA) have been used to investigate the electronic and magnetic properties of the ordered Sr_2FeMoO_6 and Sr_2FeReO_6. It has been found that at the ground state, the $Fe^{3+}(3d^5)$ is in the high spin state of $S = 5/2$ according to Hund's rule, and $Mo^{5+}(4d^1)$ and $Re^{5+}(5d^2)$ are highly ionized with valence spin states of $S = 1/2$ and $S = 1$, respectively. Each of the two TM sites, namely, the Fe^{3+} ($3d^5$, $S = 5/2$) and Mo^{5+} ($4d^1$, $S = 1/2$) or Re^{5+} ($5d^2$, $S = 1$) sites, is believed to be ferromagnetically (FM) arranged within each sublattice, while the two sublattices are coupled antiferromagnetically (AFM), giving rise to the total spin magnetic moments of 4 μ_B and 3 μ_B per formula unit (f.u.) for Sr_2FeMoO_6 and Sr_2FeReO_6, respectively. The smaller saturation magnetizations of 3 μ_B/f.u. and 2.7 μ_B/f.u. at 4.2 K for Sr_2FeMoO_6[1] and Sr_2FeReO_6[2] respectively are attributed to the mis-site-type disorder of the TM sites.[20–22]

Growth of the double perovskites Sr_2FeMoO_6 and Sr_2FeReO_6 would always lead to a certain degree of imperfections. For instance, Kobayashi *et al.*[1] found that 13% of the Fe and Mo cations in their sintered Sr_2FeMoO_6 are not on the respective sublattices. It is theoretically and experimentally shown that the ordering of the TM Fe and Mo/Re as well as the oxygen vacancy are the key factors determining the macro-

*Project supported by the National Natural Science Foundation of China (Grant No. 51501017).
†Corresponding author. E-mail: yan.zhang@chd.edu.cn
© 2016 Chinese Physical Society and IOP Publishing Ltd

scopic magnetic properties of Sr_2FeMoO_6 and Sr_2FeReO_6. The antisite defects, which are defined as the misplacement of Fe in Mo/Re positions and vice versa, and the oxygen vacancy generally decrease the saturation magnetization and the Curie temperature T_C.[1,9,10,20–32] Among those works, only Retuerto *et al.*[32] investigated the effects of the inherent imperfections on the properties of Sr_2FeReO_6 experimentally, they found that the sample prepared by a soft-chemistry technique presents 75% of Fe/Re cationic order and an enhanced Curie temperature of 445 K, while the one prepared by the high-pressure method generates a complete Fe/Re cationic order and a superior saturation magnetization. The other experimental and theoretical works on Sr_2FeReO_6 are about the external impurity substitution defects. Experimentally, Jung *et al.*[9] found that the FiM behavior of Sr_2FeReO_6 changes to the AFM upon Sb substitution. Jung *et al.*[10] studied the effects of diamagnetic dilution of the Fe sublattice on the structural and magnetic properties of $Sr_2Fe_{1-x}Ga_xReO_6$. They found that the amount of antisite disorder increases with increasing Ga content. For $0 < x < 0.4$, only a tetragonal and magnetically ordered phase is detected. A phase separation into a tetragonal phase and a cubic phase is detected for $x \geq 0.4$. The soft-chemistry method was also used by Blanco *et al.*[33] to fabricate Sr_2FeReO_6, $Sr_2FeRe_{0.9}Nb_{0.1}O_6$, and $Sr_2FeRe_{0.9}Ta_{0.1}O_6$. The lower magnetic moments compared to the theoretical ones were attributed to the antisite disorder of 25% in the B and B' positions. Blasco *et al.*[34] found that the replacement of Sr by La leads to an increase of the unit cell volume and a rise of the Curie temperature. However, both the saturated magnetic moment and the room-temperature magnetoresistance decrease with increasing La content. Theoretically, the effects of Cr substituting for Fe,[35] La substituting for Sr,[36] and Tc substituting for Re[37] on the structural, electronic, and magnetic properties of Sr_2FeReO_6 have been investigated by using the first-principles calculations within the density function theory (DFT) framework. Therefore, in this paper, on the point of view of the HM character and magnetization reduction, the structural, electronic, and magnetic properties of the imperfect double perovskite Sr_2FeReO_6 containing eight different inherent defects of Fe antisite (Fe_{Re}), Re antisite (Re_{Fe}), Fe1–Re1 interchange (Fe1–Re1), Fe1–Re4 interchange (Fe1–Re4), Fe vacancy (V_{Fe}), Re vacancy (V_{Re}), O vacancy (V_O), and Sr vacancy (V_{Sr}) are studied by using first-principles projector augmented wave (PAW) within generalized gradient approximation as well as taking into account the on-site Coulomb repulsive interaction (GGA+U).

2. Calculation method and models

The calculations are performed using the Vienna *ab initio* simulation package (VASP) based on the DFT.[38–41] The interaction between electron and ionic core is represented by the projector augmented wave (PAW) potentials,[42] which are more accurate than the ultra-soft pseudopotentials. To treat the electron exchange and correlation, we choose the Perdew–Burke–Ernzerhof (PBE)[43] formulation of the generalized gradient approximation (GGA). We take into account the on-site Coulomb repulsive interaction (GGA+U) with the effective U parameters of 2.0 eV for Fe and 1.0 eV for Re,[15,44] which yields the correct ground state structure of the strong correlation system. A conjugate-gradient algorithm is used to relax the ions into their ground states, and the energies and the forces on each ion are converged within 1.0×10^{-4} eV/atom and 0.02 eV/Å, respectively. The cutoff energy for the plane-waves is chosen to be 450 eV. The Sr $4s^24p^65s^2$, Fe $3d^64s^2$, Re $5d^56s^2$, and O $2s^22p^4$ electrons are treated as valence electrons. The k-points are sampled according to the Monkhorst–Pack automatic generation scheme with their origin at the Γ point[45] and 10 divisions in each direction, together with a Gaussian smearing broadening of 0.1 eV.

In order to compare the electronic structures of the imperfect and the perfect Sr_2FeReO_6 on the same footing, the calculations are all performed by constructing a supercell of 4 f.u. ($Sr_8Fe_4Re_4O_{24}$). As compared with Fig. 1(i) for perfect $Sr_8Fe_4Re_4O_{24}$, eight different configurations of the defects (marked with circles) are considered: (a) Fe antisite (Fe_{Re}) at (0.5, 0.5, 0.5) site ($Sr_8Fe_5Re_3O_{24}$), (b) Re antisite (Re_{Fe}) at (0, 0.5, 0.5) site ($Sr_8Fe_3Re_5O_{24}$), (c) Fe1–Re1 interchange (Fe1–Re1) at (0, 0, 0) and (0, 0, 0.5) sites ($Sr_8Fe_4Re_4O_{24}$), (d) Fe1–Re4 interchange (Fe1–Re4) at (0, 0, 0) and (0.5, 0.5, 0.5) sites ($Sr_8Fe_4Re_4O_{24}$), (e) Fe vacancy (V_{Fe}) at (0, 0.5, 0.5) site ($Sr_8Fe_3Re_4O_{24}$), (f) Re vacancy (V_{Re}) at (0.5, 0.5, 0.5) site ($Sr_8Fe_4Re_3O_{24}$), (g) O vacancy (V_O) at (0.5, 0.5, 0.25) site ($Sr_8Fe_4Re_4O_{23}$), and (h) Sr vacancy (V_{Sr}) at (0.75, 0.75, 0.75) site ($Sr_7Fe_4Re_4O_{24}$).

3. Results and discussion

3.1. Relaxed structures

The relaxed structures of 4 f.u. Sr_2FeReO_6 with eight different defects (marked with circles) are shown in Figs. 1(a)–1(h) together with the perfect one in Fig. 1(i) for comparison. From Figs. 1(a)–1(d), we can see that, for Fe_{Re}, Re_{Fe} antisites and Fe1–Re1, Fe1–Re4 interchanges cases, no obvious structural changes are observed due to the Fe^{3+} and Re^{5+} ions having similar radii of 0.78 Å and 0.72 Å,[46] respectively. However, from Figs. 1(e) and 1(f), we can see that, for V_{Fe}/V_{Re} vacancy cases, the vanished attractions of the removed Fe/Re atom make its six nearest neighbor oxygen atoms move close to their nearest Re/Fe neighbors, so the corresponding Re–O/Fe–O bond lengths reduce to 1.881 Å/1.798 Å. While in perfect Sr_2FeReO_6, the optimized bond lengths are 1.937 Å/2.008 Å for Re–O/Fe–O bonds, as shown in Fig. 1(i). Figure 1(g) shows that the vanished repulsive forces of the removed oxygen atom make its eight

nearest neighbor oxygen atoms move close to the V_O vacancy site. Figure 1(h) shows that there are no obvious structural changes for the V_{Sr} vacancy case. As mentioned in our previous paper,[47] this is because the interactions between the Sr atom and its nearest neighbor atoms are very weak due to the completely filled Sr 4p and 5s subshells.

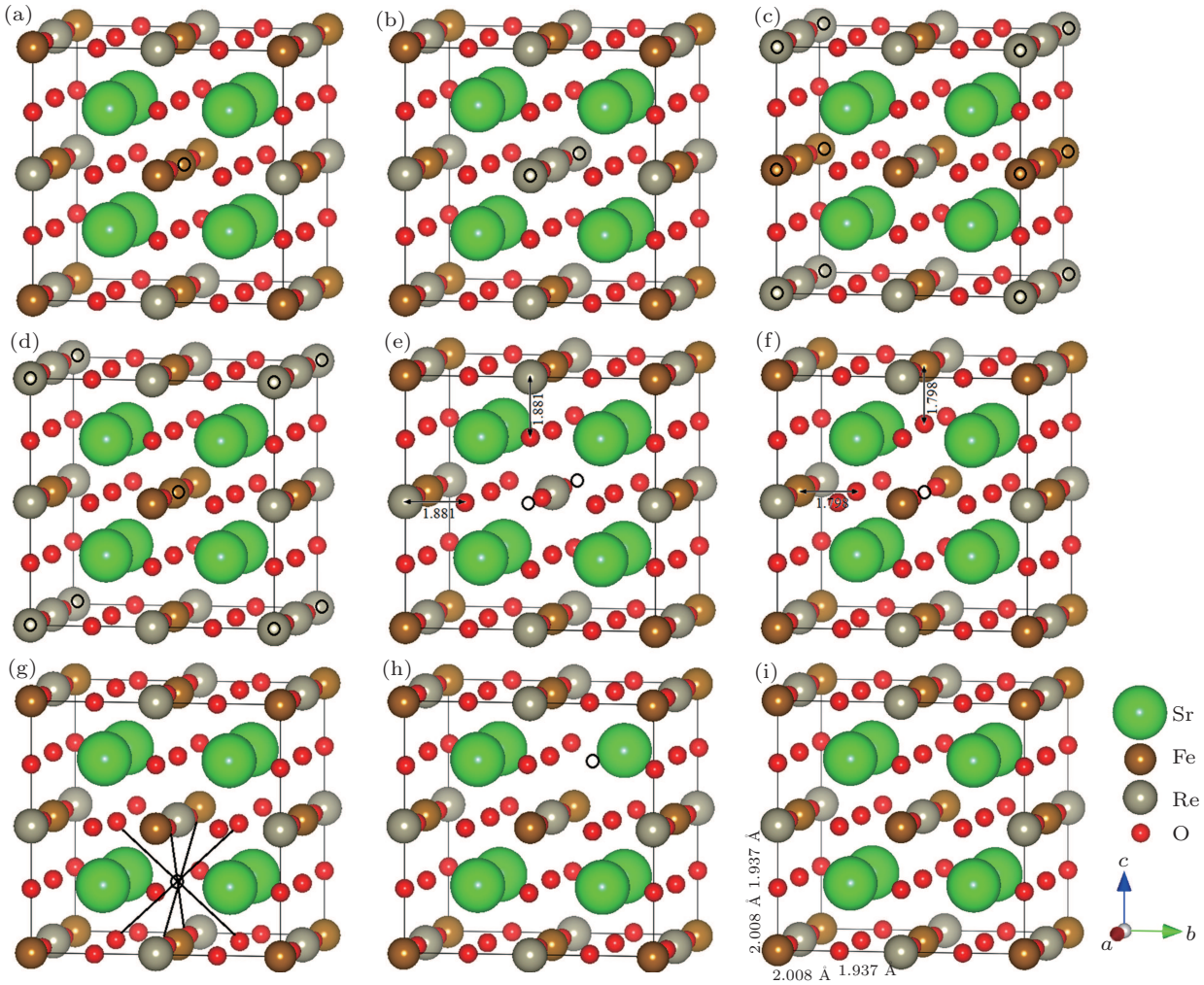


Fig. 1. (color online) Optimized structures of imperfect (marked with circles) Sr_2FeReO_6 of 4 f.u. containing (a) Fe antisite (Fe_{Re}), one Fe atom substituting for one Re atom at (0.5, 0.5, 0.5) site ($Sr_8Fe_5Re_3O_{24}$), (b) Re antisite (Re_{Fe}), one Re atom substituting for one Fe atom at (0, 0.5, 0.5) site ($Sr_8Fe_3Re_5O_{24}$), (c) Fe1–Re1 interchange (Fe1–Re1), exchanging Fe and Re positions respectively at (0, 0, 0) and (0, 0, 0.5) sites ($Sr_8Fe_4Re_4O_{24}$), (d) Fe1–Re4 interchange (Fe1–Re4), exchanging Fe and Re positions respectively at (0, 0, 0) and (0.5, 0.5, 0.5) sites ($Sr_8Fe_4Mo_4O_{24}$), (e) Fe vacancy (V_{Fe}), removing one Fe atom from (0, 0.5, 0.5) site ($Sr_8Fe_3Re_4O_{24}$), (f) Re vacancy (V_{Re}), removing one Re atom from (0.5, 0.5, 0.5) site ($Sr_8Fe_4Re_3O_{24}$), (g) O vacancy (V_O), removing one O atom from (0.5, 0.5, 0.25) site ($Sr_8Fe_4Re_4O_{23}$), and (h) Sr vacancy (V_{Sr}), removing one Sr atom from (0.75, 0.75, 0.75) site ($Sr_7Fe_4Re_4O_{24}$). The optimized structure of the perfect Sr_2FeReO_6 of 4 f.u. ($Sr_8Fe_4Re_4O_{24}$) is also shown in panel (i) for comparison.

3.2. HM characters

In order to investigate the effects of the defects on the HM character of the double perovskite Sr_2FeReO_6, which are very important for its application in spintronic devices, we show in Fig. 2 the total density of states (DOS) of 4 f.u. Sr_2FeReO_6 containing eight different defects of (a) Fe antisite (Fe_{Re}), (b) Re antisite (Re_{Fe}), (c) Fe1–Re1 interchange (Fe1–Re1), (d) Fe1–Re4 interchange (Fe1–Re4), (e) Fe vacancy (V_{Fe}), (f) Re vacancy (V_{Re}), (g) O vacancy (V_O), or (h) Sr vacancy (V_{Sr}). We can see that, the HM characters are maintained for imperfect Sr_2FeReO_6 containing (a) Fe_{Re} antisite, (b) Re_{Fe} antisite, (d) Fe1–Re4 interchange, (e) V_{Fe} vacancy, (g) V_O vacancy, or (h) V_{Sr} vacancy, because their down-spin channels (red lines) cross the Fermi level E_F and the up-spin channels (black lines) open the band gaps $E_g^{up-spin}$ of 0.614 eV, 0.769 eV, 0.757 eV, 1.371 eV, 1.527 eV, and 1.535 eV, respectively. On the contrary, the HM characters are lost for imperfect Sr_2FeReO_6 containing (c) Fe1–Re1 interchange and (f) V_{Re} vacancy, since the total DOS of both down-spin (red lines) and up-spin (black lines) channels cross the Fermi level E_F. The HM characters of the imperfect Sr_2FeReO_6 are lost for (c) Fe1–Re1 interchange at (0, 0, 0) and (0, 0, 0.5) sites but maintained for (d) Fe1–Re4 interchange at (0, 0, 0) and (0.5, 0.5, 0.5) sites, because the separation distance of 3.945 Å for Fe1–Re1 interchange is smaller than that of 6.833 Å for Fe1–Re4 interchange. So we conclude that the near Fe1–Re1 interchange and V_{Re} vacancy defects should be avoided in order to preserve the HM characters of the Sr_2FeReO_6 and thus usage in spintronic devices.

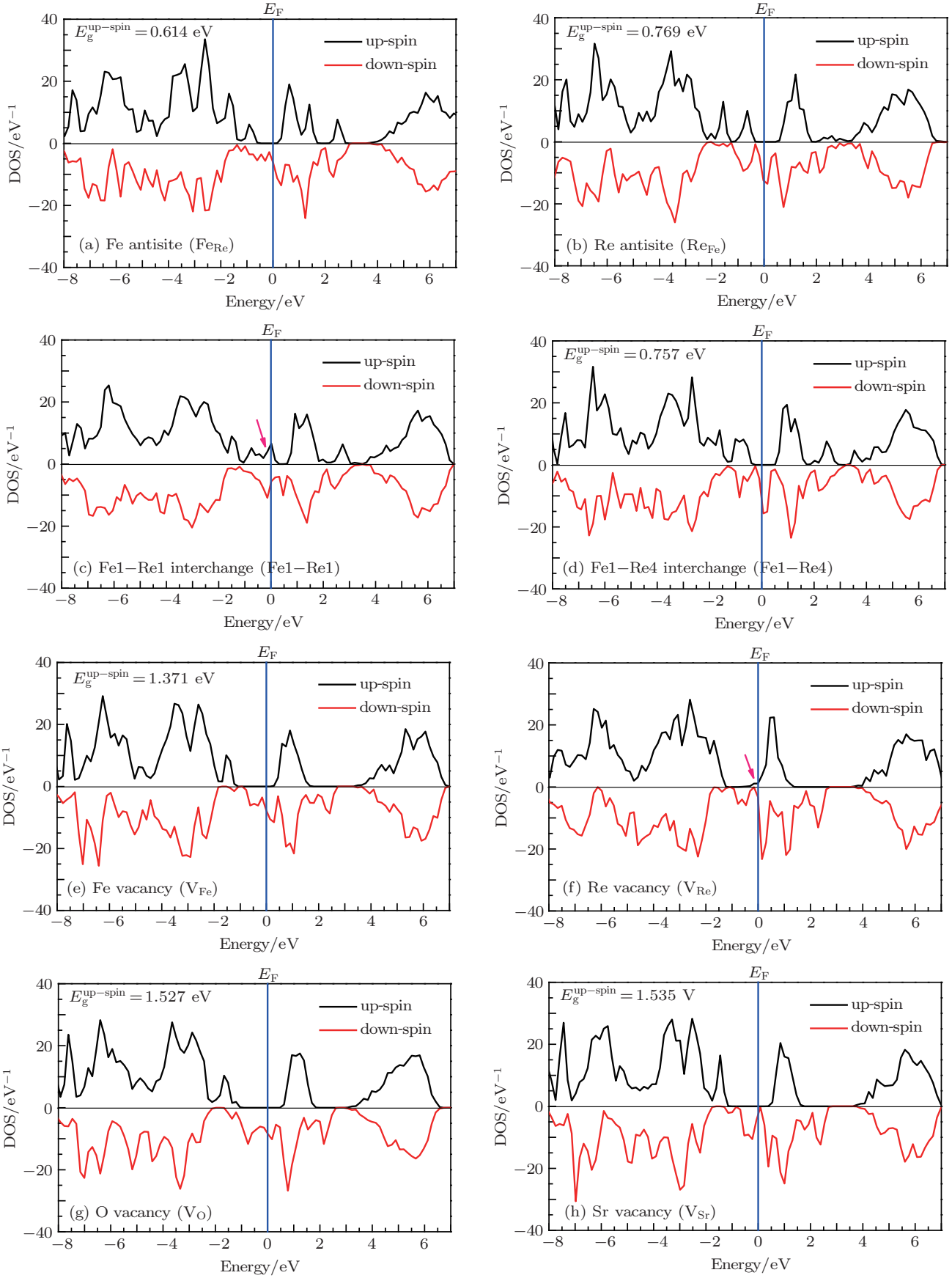


Fig. 2. (color online) Total density of states (DOS) of imperfect Sr_2FeReO_6 of 4 f.u. containing (a) Fe antisite (Fe_{Re}), (b) Re antisite (Re_{Fe}), (c) Fe1–Re1 interchange (Fe1–Re1), (d) Fe1–Re4 interchange (Fe1–Re4), (e) Fe vacancy (V_{Fe}), (f) Re vacancy (V_{Re}), (g) O vacancy (V_O), or (h) Sr vacancy (V_{Sr}). The black and red lines represent up-spin and down-spin DOS, respectively, and the Fermi level E_F is set at zero energy and indicated by the vertical blue lines.

Now we turn to examine the disappearing reason of the HM character of the imperfect Sr_2FeReO_6 containing Fe1–Re1 interchange defect (see Figs. 1(c) and 2(c) for the structure and the total DOS). The detailed orbital-decomposed density of states (ODDOS) projected onto the concerned inequivalent Fe atoms at (0, 0, 0.5) Fe_{Re} antisite and (0.5, 0.5, 0) regular Fe site and Re atoms at (0, 0, 0) Re_{Fe} antisite and (0.5, 0.5, 0.5) regular Re site is shown in Fig. 3. It is clear that the total DOS of the down-spin channel (red line) crossing the Fermi level E_F in Fig. 2(c) for the imperfect Sr_2FeReO_6 containing the Fe1–Re1 interchange defect resulted from the hybridizations of the t_{2g} (d_{xy}, d_{yz} and d_{zx}) states of the Fe and Re atoms at regular sites and antisites, while the occurrence of the up-spin state (marked with an arrow in Fig. 2(c)) in the band gap region of the perfect Sr_2FeReO_6, i.e., the disappearing reason of the HM character of the imperfect Sr_2FeReO_6 containing the Fe1–Re1 interchange defect, is attributed to the small bonding-antibonding splitting of the up-spin t_{2g} (d_{xy}, d_{yz} and d_{zx}) states of both antisite Re_{Fe} at (0, 0, 0) (especially) and near antisite Fe_{Re} at (0, 0, 0.5) with positive and negative magnetic moments, respectively. It should be pointed out that such a small bonding-antibonding splitting of the up-spin t_{2g} (d_{xy}, d_{yz} and d_{zx}) states also exists in the other imperfect Sr_2FeReO_6 with HM character, it is just because the split bonding state and the antibonding state of the up-spin t_{2g} (d_{xy}, d_{yz} and d_{zx}) orbitals do not cross the Fermi level E_F and thus open the various up-spin band gaps $E_g^{up-spin}$ (eV) as mentioned above.

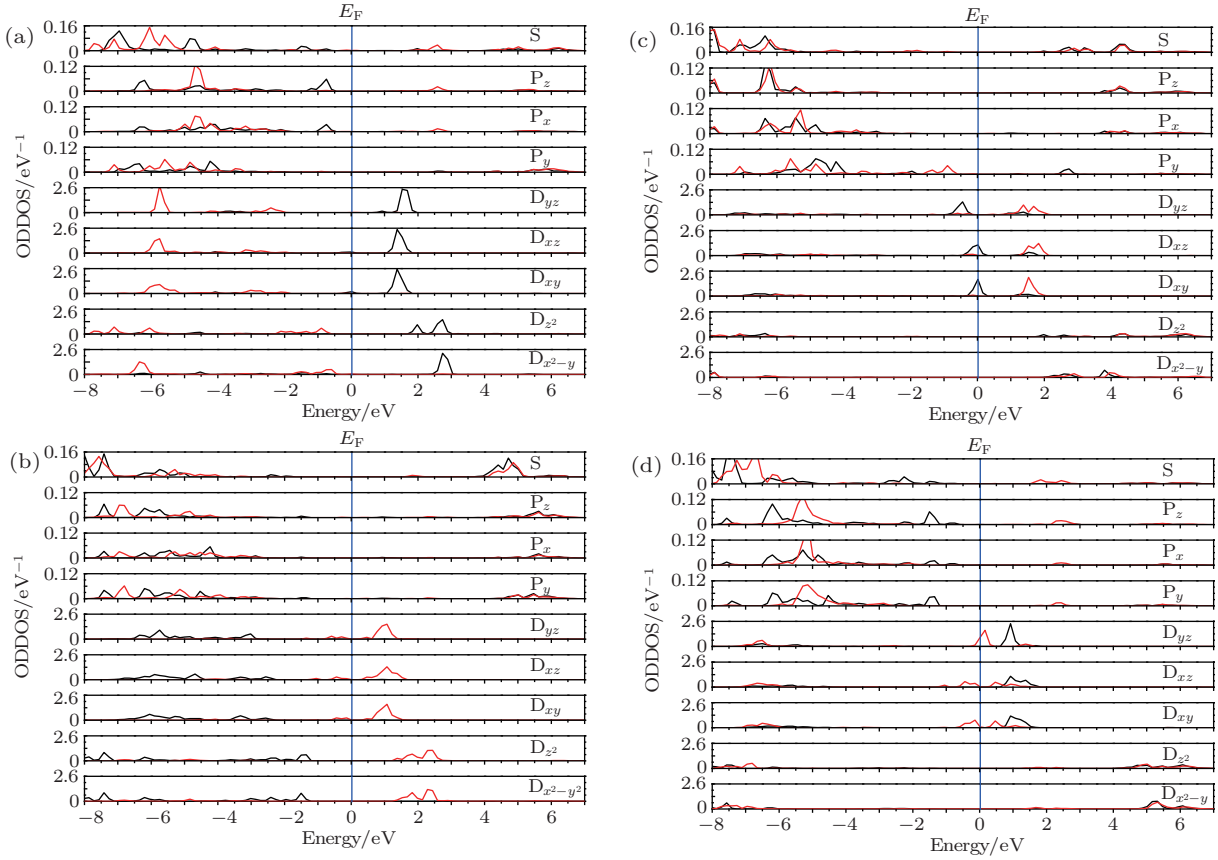


Fig. 3. (color online) Orbital-decomposed density of states (ODDOS) projected onto the concerned inequivalent Fe atoms at (a) (0, 0, 0.5) Fe_{Re} antisite and (b) (0.5, 0.5, 0) regular Fe site and Re atoms at (c) (0, 0, 0) Re_{Fe} antisite and (d) (0.5, 0.5, 0.5) regular Re site for imperfect Sr_2FeReO_6 containing the Fe1–Re1 interchange defect (see Figs. 1(c) and 2(c) for the structure and the total DOS). The black and red lines represent up-spin and down-spin DOS, respectively, and the Fermi level E_F is set at zero energy and indicated by the vertical blue lines.

3.3. Spin couplings and magnetic moments

In order to investigate the effects of the defects on the spin coupling and magnetic moments, we show the spin or difference charge densities ($\rho_{spin} = \rho_{up-spin} - \rho_{down-spin}$) in Fig. 4 for imperfect 4 f.u. Sr_2FeReO_6 containing eight different defects of (a) Fe antisite (Fe_{Re}) at (0.5, 0.5, 0.5) site, (b) Re antisite (Re_{Fe}) at (0, 0.5, 0.5) site, (c) Fe1–Re1 interchange (Fe1–Re1) at (0, 0, 0) and (0, 0, 0.5) sites, (d) Fe1–Re4 interchange (Fe1–Re4) at (0, 0, 0) and (0.5, 0.5, 0.5) sites, (e) Fe vacancy (V_{Fe}) at (0, 0.5, 0.5) site, (f) Re vacancy (V_{Re}) at (0.5, 0.5, 0.5) site, (g) O vacancy (V_O) at (0.5, 0.5, 0.25) site, or (h) Sr vacancy (V_{Sr}) at (0.75, 0.75, 0.75) site. The spin charge density of the perfect 4 f.u. Sr_2FeReO_6 is also shown in Fig. 4(i) for comparison. The yellow (turquoise) isosurfaces represent the positive (negative) charge density of 0.005 e/Å^3 and thus an up-spin (down-spin) moment. In the (100) cross

sections, the colors blue, turquoise, and green represent the values of spin charge density in increasing order. We can see that, firstly, in cases of (a) Fe_{Re} antisite at (0.5, 0.5, 0.5) site, (b) Re_{Fe} antisite at (0, 0.5, 0.5) site, (c) Fe1–Re1 interchange at (0, 0, 0) and (0, 0, 0.5) sites, and (d) Fe1–Re4 interchange at (0, 0, 0) and (0.5, 0.5, 0.5) sites (each interchange contains one Fe_{Re} antisite pluses one Re_{Fe} antisite), the spin moments of the Fe (Re) cations situated on Re (Fe) antisites are coupled AFM with those of the Fe (Re) cations on the regular sites. We also make an FM configuration calculation for each case, i.e., all the Fe (Re) moments are positive (negative), but the total energies are 2.67 eV, 0.00 eV (in fact pushed to the AFM configuration), 0.36 eV, and 0.49 eV higher than the AFM ground states for the (a) Fe_{Re} antisite, (b) Re_{Fe} antisite, (c) Fe1–Re1 interchange, and (d) Fe1–Re4 interchange cases, respectively. Secondly, in cases of (e) V_{Fe} vacancy, (f) V_{Re} vacancy, (g) V_O vacancy, and (h) V_{Sr} vacancy, an FM coupling is observed within each cation sublattice, while the two cation sublattices are AFM coupled. This is similar to the perfect Sr_2FeReO_6 case shown in Fig. 4(i). Thirdly, as expected, each cation defect affects mainly its six nearest neighbor oxygen atoms. In cases of (a) Fe_{Re} antisite, (c) Fe1–Re1 interchange, (d) Fe1–Re4 interchange, (e) V_{Fe} vacancy, and (f) V_{Re} vacancy, a partial negative spin moment (turquoise) presents on the six nearest neighbor oxygen atoms, while in the Re_{Fe} antisite case (b), no spin moments are observed on the six nearest neighbor oxygen atoms. Fourthly, the V_O vacancy at (0.5, 0.5, 0.25) site causes the nearest neighbor Re4 cation at central (0.5, 0.5, 0.5) site having a much larger and expansive negative spin moment (turquoise) and its five survived nearest neighbor oxygen atoms having a partial negative spin moment (turquoise). Finally, no spin density distributions at eight Sr sites in cases (a)–(g) and no obvious influence on the magnetic moment distributions in case (h) both indicate that the contributions to the magnetic moment from the Sr atoms are neglectable.

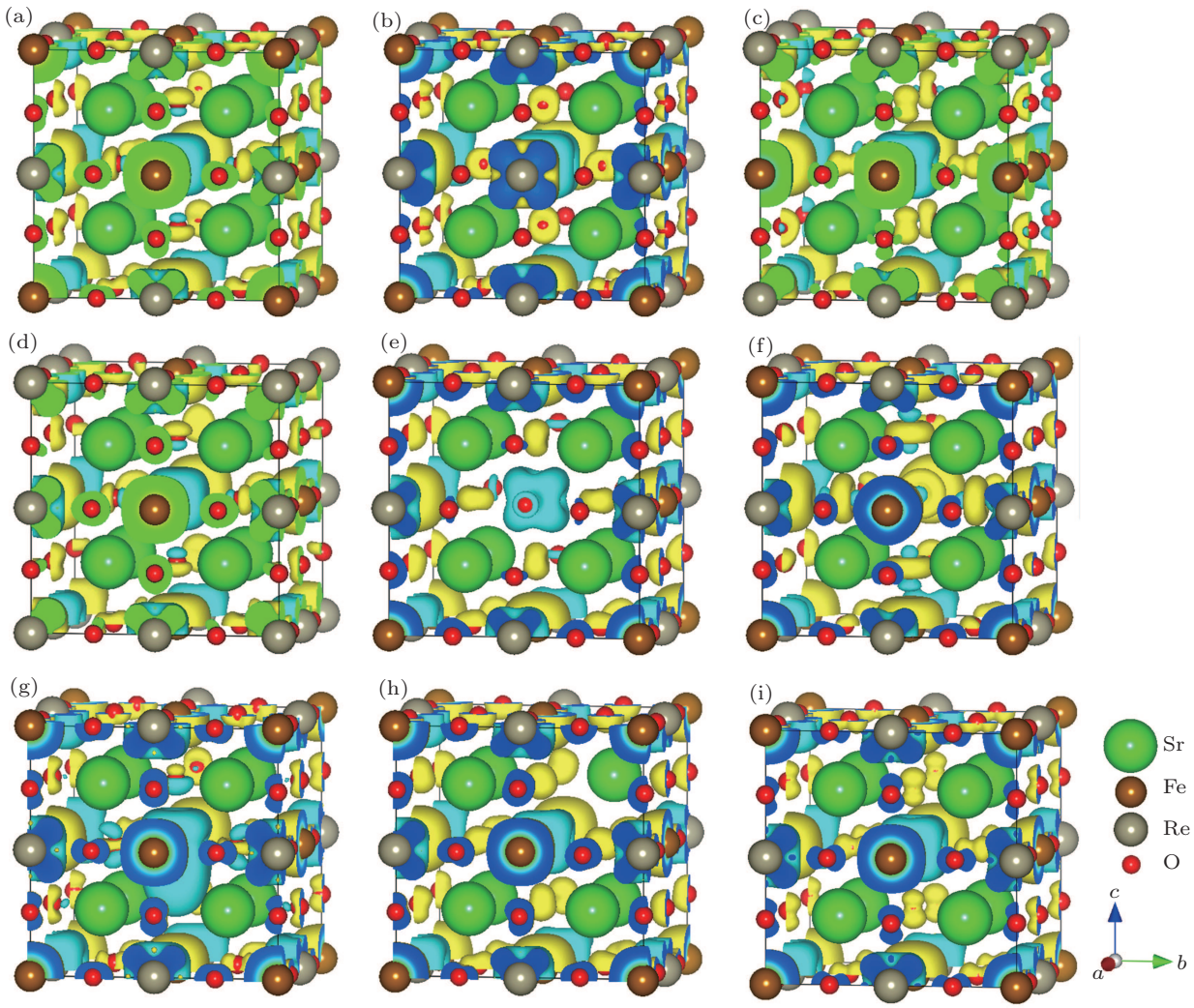


Fig. 4. (color online) The spin charge density of imperfect Sr_2FeReO_6 of 4 f.u. containing (a) Fe antisite (Fe_{Re}) at (0.5, 0.5, 0.5) site, (b) Re antisite (Re_{Fe}) at (0, 0.5, 0.5) site, (c) Fe1–Re1 interchange (Fe1–Re1) at (0, 0, 0) and (0, 0, 0.5) sites, (d) Fe1–Re4 interchange (Fe1–Re4) at (0, 0, 0) and (0.5, 0.5, 0.5) sites, (e) Fe vacancy (V_{Fe}) at (0, 0.5, 0.5) site, (f) Re vacancy (V_{Re}) at (0.5, 0.5, 0.5) site, (g) O vacancy (V_O) at (0.5, 0.5, 0.25) site, or (h) Sr vacancy (V_{Sr}) at (0.75, 0.75, 0.75) site. The spin charge density of the perfect Sr_2FeReO_6 of 4 f.u. is also shown in panel (i) for comparison. The yellow (turquoise) isosurfaces represent positive (negative) charge density of 0.005 $e/Å^3$ and thus an up-spin (down-spin) moment. In the (100) cross sections, the colors blue, turquoise, and green represent the values of spin charge density in increasing order.

The initial fractional coordinates (x, y, z) and local magnetic moments μ (μ_B) of the Fe and Re atoms on the regular site and antisites, the total magnetic moments μ_{tot} (μ_B/f.u.), the HM characters, and the up-spin band gaps $E_g^{up-spin}$ (eV) of the imperfect 4 f.u. Sr_2FeReO_6 containing eight different defects are summarized in Table 1, together with the values of the perfect Sr_2FeReO_6 for comparison. It is clearly shown that, except for the V_{Re} and V_{Sr} vacancy cases, the total magnetic moment μ_{tot} of the imperfect Sr_2FeReO_6 system with one of the other six different defects is smaller than that of the perfect one. So the smaller measured saturation magnetization of 2.7 μ_B/f.u. at 4.2 K in Sr_2FeReO_6[2] compared to the theoretical value of 3.0 μ_B/f.u. can be attributed to various defects. Furthermore, from Table 1, we can see that for the Fe_{Re} antisite case, the reduced saturation magnetization is resulted from the occurrence of antiparallel aligned magnetic moment -3.926 μ_B on Fe_{Re} antisite. For the Re_{Fe} antisite case, the reduced saturation magnetization is attributed to the fact that the supplied parallel aligned magnetic moment 1.561 μ_B by the Re_{Fe} antisite is smaller than the disappeared moment 3.696 μ_B of the substituted Fe. These two reducing magnetization mechanisms occur simultaneously in the Fe1–Re1 (Fe1–Re4) interchange cases, i.e. antiparallel aligned magnetic moments -3.929 μ_B (-3.915 μ_B) on Fe_{Re} antisites and supplied smaller parallel aligned magnetic moments 1.353 μ_B (1.400 μ_B) by Re_{Fe} antisites, leading to the much lower saturation magnetizations of 1.87 μ_B/f.u. (1.96 μ_B/f.u.). The vanishing of a regular site Fe atom and thus the vanishing of its parallel aligned magnetic moment (3.696 μ_B) is clearly responsible for the reduced saturation magnetization of the imperfect Sr_2FeReO_6 with V_{Fe} vacancy. Although removing a Re atom from its regular sublattice leads to decreasing parallel aligned magnetic moments on its three near Fe2, Fe3, and Fe4 neighbors, both the vanishing (decreasing) antiparallel aligned magnetic moment on itself (its three near Re1, Re2, and Re3 neighbors) and a slightly increasing parallel aligned magnetic moment on the Fe1 atom result in a larger saturation magnetization of 3.43 μ_B/f.u. in imperfect Sr_2FeReO_6 with V_{Re} vacancy. Although removing an oxygen atom causes slightly increasing parallel aligned magnetic moments on four Fe atoms on the regular sublattice, both the vanishing parallel aligned magnetic moment and especially the increasing antiparallel aligned magnetic moments on the four Re atoms on the regular sublattice still lead to the slightly smaller saturation magnetization of 2.64 μ_B/f.u. in the imperfect Sr_2FeReO_6 containing V_O vacancy. Finally, the total magnetic moment μ_{tot} of the imperfect Sr_2FeReO_6 with V_{Sr} vacancy is larger than that of the perfect one. The reason is that not only the parallel aligned magnetic moment of about 3.90 μ_B for four Fe atoms is larger than that of 3.696 μ_B for four Fe atoms in perfect Sr_2FeReO_6, but also the antiparallel aligned magnetic moment of about -0.71 μ_B for four Re atoms is smaller than that of -0.857 μ_B for four Re atoms in perfect Sr_2FeReO_6, so the largest saturation magnetization of 3.50 μ_B/f.u. is found.

Table 1. The initial fractional coordinates (x, y, z) and local magnetic moments μ (μ_B) of the Fe and Re atoms on the regular site and antisites, the total magnetic moments μ_{tot} (μ_B/f.u.), half-metallic characters, and up-spin band gaps $E_g^{up-spin}$ (eV) of imperfect 4 f.u. Sr_2FeReO_6 containing eight different defects. The values corresponding to the perfect Sr_2FeReO_6 are also shown for comparison.

	Coordinates (x, y, z)	Fe antisite (Fe_{Re})	Re antisite (Re_{Fe})	Fe1–Re1 interchange (Fe1–Re1)	Fe1–Re4 interchange (Fe1–Re4)	Fe vacancy (V_{Fe})	Re vacancy (V_{Re})	O vacancy (V_O)	Sr vacancy (V_{Sr})	Perfect
Fe	Fe1(0, 0, 0)	3.910	3.926	Re_{Fe}	Re_{Fe}	3.868	3.970	3.901	3.889	3.696
	Fe2(0, 0.5, 0.5)	3.953	Re_{Fe}	3.925	3.962	V_{Fe}	3.265	3.886	3.905	3.696
	Fe3(0.5, 0, 0.5)	3.919	3.927	3.950	3.936	3.954	3.177	3.918	3.905	3.696
	Fe4(0.5, 0.5, 0)	3.884	3.916	3.921	3.912	3.862	3.131	3.733	3.898	3.696
	Fe_{Re}(0.5,0.5,0.5)	-3.926 Fe_{Re}			-3.915 Fe_{Re}					
	Fe_{Re}(0, 0, 0.5)			-3.929 Fe_{Re}						
Re	Re1(0, 0, 0.5)	-0.548	–1.192	Fe_{Re}	–0.670	–0.594	–0.396	–1.156	–0.714	–0.857
	Re2(0, 0.5, 0)	–0.578	–1.161	–0.763	–0.781	–0.650	–0.376	–1.254	–0.712	–0.857
	Re3(0.5, 0, 0)	–0.630	–1.210	–0.847	–0.831	–0.576	–0.398	–1.276	–0.712	–0.857
	Re4(0.5,0.5,0.5)	Fe_{Re}	–1.246	–0.891	Fe_{Re}	–0.596	V_{Re}	–1.546	–0.715	–0.857
	Re_{Fe}(0, 0.5, 0.5)		1.561 Re_{Fe}							
	Re_{Fe}(0, 0, 0)			1.353 Re_{Fe}	1.400 Re_{Fe}					
μ_{tot}/μ_B		2.74	2.29	1.87	1.96	2.51	3.43	2.64	3.50	3.00
HM character		yes	yes	no	yes	yes	no	yes	yes	yes
$E_g^{up-spin}$/eV		0.614	0.769	–	0.757	1.371	–	1.527	1.535	0.46

4. Conclusion

From the aspects of HM character and magnetization reduction, the structural, electronic, and magnetic properties of the imperfect Sr_2FeReO_6 containing eight different defects of Fe_{Re} or Re_{Fe} antisites, Fe1–Re1 or Fe1–Re4 interchanges, V_{Fe}, V_{Re}, V_O, or V_{Sr} vacancies have been studied by using the first-principles projector augmented wave (PAW) potential within the generalized gradient approximation as well as taking into account on-site the Coulomb repulsive interaction (GGA+U). The following results have been obtained.

(i) No obvious structural changes are observed for the imperfect Sr_2FeReO_6 containing Fe_{Re} or Re_{Fe} antisites, Fe1–Re1

or Fe1–Re4 interchanges, or V_{Sr} vacancy defects. However, the six (eight) nearest oxygen neighbors of the vacancy move away from (close to) V_{Fe} or V_{Re} (V_O) vacancies.

(ii) The HM character is maintained for the imperfect Sr_2FeReO_6 containing Fe_{Re} or Re_{Fe} antisites, Fe1–Re4 interchange, V_{Fe}, V_O, or V_{Sr} vacancies, while it vanishes when Fe1–Re1 interchange or V_{Re} vacancy is presented. So the Fe1–Re1 interchange and V_{Re} vacancy defects should be avoided to preserve the HM character of the Sr_2FeReO_6 and thus usage in spintronic devices.

(iii) In Fe_{Re} or Re_{Fe} antisites, Fe1–Re1 or Fe1–Re4 interchanges cases, the spin moments of the Fe (Re) cations situated on Re (Fe) antisites are in an antiferromagnetic coupling with those of the Fe (Re) cations on the regular sites. In V_{Fe}, V_{Re}, V_O, or V_{Sr} vacancy cases, a ferromagnetic coupling is obtained within each cation sublattice, while the two cation sublattices are coupled antiferromagnetically.

(iv) The total magnetic moments μ_{tot} (μ_B/f.u.) of the imperfect Sr_2FeReO_6 containing eight different defects decrease in the sequence of V_{Sr} vacancy (3.50), V_{Re} vacancy (3.43), Fe_{Re} antisite (2.74), V_O vacancy (2.64), V_{Fe} vacancy (2.51), Re_{Fe} antisite (2.29), Fe1–Re4 interchange (1.96), Fe1–Re1 interchange (1.87), and the mechanisms of the saturation magnetization reduction have been discussed.

References

[1] Kobayashi K I, Kimura T, Sawada H, Terakura K and Tokura Y 1998 *Nature* **395** 677

[2] Kobayashi K I, Kimura T, Tomioka Y, Sawada H, Terakura K and Tokura Y 1999 *Phys. Rev. B* **59** 11159

[3] Rao C N R and Raveau B 1998 *Colossal Magnetoresistance, Charge Ordering and Related Properties of Manganese Oxides* (Singapore: World Scientific Publishers)

[4] Wolf S A, Awschalom D D, Buhrman R A, Daughton J M, Molnár S V, Roukes M L, Chtchelkanova A Y and Treger D M 2001 *Science* **294** 1488

[5] Tomioka Y, Okuda T, Okimoto Y, Kumai R, Kobayashi K I and Tokura Y 2000 *Phys. Rev. B* **61** 422

[6] Chmaissem O, Kruk R, Dabrowski B, Brown D E, Xiong X, Kolesnik S, Jorgensen J D and Kimball C W 2000 *Phys. Rev. B* **62** 14197

[7] Navarro J, Frontera C, Balcells L, Martínez B and Fontcuberta J 2001 *Phys. Rev. B* **64** 092411

[8] Moreno M S, Gayone J E, Abbate M, Caneiro A, Niebieskikwiat D, Sánchez R D, Siervo A de, Landers R and Zampieri G 2002 *Physica B* **320** 43

[9] Jung A, Ksenofontov V, Reiman S, Therese H A, Kolb U, Felser C and Tremel W 2006 *Phys. Rev. B* **73** 144414

[10] Jung A, Bonn I, Ksenofontov V, Panthöfer M, Reiman S, Felser C and Tremel W 2007 *Phys. Rev. B* **75** 184409

[11] Ohno K, Kato H, Nishioka T and Matsumura M 2007 *J. Magn. Magn. Mater.* **310** e666

[12] Hu Y C, Ge J J, Ji Q, Jiang Z S, Wu X S and Cheng G F 2010 *Mater. Chem. Phys.* **124** 274

[13] Pan Y W, Zhu P W and Wang X 2015 *Chin. Phys. B* **24** 017503

[14] Sarma D D, Mahadevan P, Saha-Dasgupta T, Ray S and Kumar A 2000 *Phys. Rev. Lett.* **85** 2549

[15] Moritomo Y, Xu Sh, Akimoto T, Machida A, Hamada N, Ohoyama K, Nishibori E, Takata M and Sakata M 2000 *Phys. Rev. B* **62** 14224

[16] Fang Z, Terakura K and Kanamori J 2001 *Phys. Rev. B* **63** 180407

[17] Wu H 2001 *Phys. Rev. B* **64** 125126

[18] Solovyev I V 2002 *Phys. Rev. B* **65** 144446

[19] Jeng H T and Guo G Y 2003 *Phys. Rev. B* **67** 094438

[20] Saha-Dasgupta T and Sarma D D 2001 *Phys. Rev. B* **64** 064408

[21] Ogale A S, Ogale S B, Ramesh R and Venkatesan T 1999 *Appl. Phys. Lett.* **75** 537

[22] Ray S, Kumar A, Sarma D D, Cimino R, Turchini S, Zennaro S and Zema N 2001 *Phys. Rev. Lett.* **87** 097204

[23] Munoz-García A B, Pavone M and Carter E A 2011 *Chem. Mater.* **23** 4525

[24] Kircheisen R and Töpfer J 2012 *J. Solid State Chem.* **185** 76

[25] Meneghini C, Ray S, Liscio F, Bardelli F, Mobilio S and Sarma D D 2009 *Phys. Rev. Lett.* **103** 046403

[26] Balcells L, Navarro J, Bibes M, Roig A, Martinez B and Fontcuberta J 2001 *Appl. Phys. Lett.* **78** 781

[27] Zhu X F, Li Q F and Chen L F 2007 *Solid State Commun.* **144** 230

[28] Stoeffler D and Colis S 2005 *J. Magn. Magn. Mater.* **290–291** 400

[29] Stoeffler D and Colis S 2006 *Mater. Sci. Eng. B* **126** 133

[30] Stoeffler D and Etz C 2006 *J. Phys.: Condens. Matter* **18** 11291

[31] Frontera C and Fontcuberta J 2004 *Phys. Rev. B* **69** 014406

[32] Retuerto M, Martínez-Lope M J, García-Hernández M and Alonso J A 2009 *Mater. Res. Bull.* **44** 1261

[33] Blanco J J, Insausti M, Lezama L, Chapman J P, Gil de Muro I and Rojo T 2004 *J. Solid State Chem.* **177** 2749

[34] Blasco J, Rodríguez-Velamazán J A, Ritter C, Sesé J, Stankiewicz J and Herrero-Martín J 2009 *Solid State Sci.* **11** 1535

[35] Li Q F, Zhu X F and Chen L F 2008 *Phys. Lett. A* **372** 2911

[36] Li Q F, Wang L and Su J L 2011 *Mod. Phys. Lett. B* **25** 2259

[37] Wang J, Zhang J M, Wang S F and Xu K W 2013 *J. Magn. Magn. Mater.* **329** 30

[38] Kresse G and Hafner J 1993 *Phys. Rev. B* **47** 558

[39] Kresse G and Hafner J 1994 *Phys. Rev. B* **49** 14251

[40] Kresse G and Furthmüller J 1996 *Comput. Mater. Sci.* **6** 15

[41] Kresse G and Furthmüller J 1996 *Phys. Rev. B* **54** 11169

[42] Kresse G and Joubert D 1999 *Phys. Rev. B* **59** 1758

[43] Perdew J P, Burke K and Ernzerhof M 1996 *Phys. Rev. Lett.* **77** 3865

[44] Saitoh T, Nakatake M, Kakizaki A, Nakajima H, Morimoto O, Xu Sh, Moritomo Y, Hamada N and Aiura Y 2002 *Phys. Rev. B* **66** 035112

[45] Monkhorst H J and Pack J D 1976 *Phys. Rev. B* **13** 5188

[46] Shannon R D 1976 *Acta Cryst. A* **32** 751

[47] Zhang Y and Ji V 2012 *Physica B* **407** 912